



Effects of aging on mechanical properties and microstructure of multi-directionally forged 7075 aluminum alloy

Tomoya Aoba*, Masakazu Kobayashi, Hiromi Miura

Department of Mechanical Engineering, Toyohashi University of Technology, 1-1 Tempaku-cho, Toyohashi, Aichi 441-8580, Japan

ARTICLE INFO

Keywords:

Aluminum alloy
Aging
Precipitation
Strength
Severe plastic deformation
Multi-directional forging

ABSTRACT

The effects of natural aging for a long period of time (2.4 years) and as well as artificial aging on the mechanical properties and microstructure of multi-directionally forged (MDFed) 7075 aluminum alloys were systematically investigated. MDFing up to a cumulative strain of 0.7 increased yield strength (+96 MPa) and ultimate tensile strength (+94 MPa) mainly due to work hardening. The addition of both natural aging at ambient temperature for 7800 ks and artificial aging at 393 K for 26 ks of the MDFed samples further increased yield strength (+190 MPa) and (+293 MPa), respectively. The microstructure and mechanical properties derived by MDFing were stably maintained for a long period of time during natural aging, even while distinct softening took place soon after the commencement of artificial aging. The number of precipitates in the MDFed samples after natural aging was notably smaller compared with that introduced by artificial aging. The achieved strengths after aging were, therefore, almost comparable.

1. Introduction

7075 aluminum alloy (7075Al) is one of the major types possessing ultimate high strength and is typically employed for structural parts that require a high strength-to-weight ratio performance such as in aircraft and other transportation applications. Improvement in the mechanical properties of this alloy can be achieved by age hardening, which is caused by homogeneously distributed fine precipitates [1]. The most common precipitation process performed during the aging heat treatment in Al-Zn-Mg-Cu alloys is as follows; supersaturated solid-solution state → coherent Guinier-Preston (GP) zones → semi-coherent η' phase → incoherent η phase [2]. Vacancy-rich clusters retained after quick quenching serve as possible nuclei for precipitates [3]. Two-step aging is the most widely employed process for Al-Zn-Mg-Cu alloys with lower temperature aging during the first step of the process enabling homogeneous dispersion of fine GP zones or clusters followed by coarsening or transformation of them in the second step of aging at higher temperatures [4]. Therefore, the control of size and distribution of precipitates are key factors for strengthening in Al-Zn-Mg-Cu alloys.

Another effective method to improve the mechanical properties of Al alloys is grain refinement. In particular, several severe plastic deformation (SPD) methods, which can produce ultrafine grained microstructures [5], have attracted significant attention in recent years. SPD methods were applied to 7075Al and the yield strength was significantly improved to 645 MPa by equal-channel angular pressing

(ECAP) [6], 550 MPa by high-pressure sliding (HPS) [7] and ~1 GPa by high pressure torsion (HPT) [8]. In these cases, ultrafine grained (UFGed) structures with average grain sizes from 26 to 600 nm were achieved. To further enhance the strength of UFGed 7075Al, age-hardening should be employed. Aging of SPDed materials at conventional aging temperatures, however, appears less effective because of their thermal instability which causes recovery followed by grain growth [9–11]. Such microstructural changes spoil the mechanical properties of the SPDed materials. The aging process of the SPDed materials, therefore, remains an open research problem [9–11]. Nevertheless, some influential rules are proposed [11]. A lower aging temperature compared with a conventional one would be favorable for age hardening after SPD to prevent recovery and grain growth. However, as far as the authors know there are few researches concerned with the effects of long-term aging on the mechanical properties and microstructure of SPDed aluminum alloys.

Multi-directional forging (MDFing) is one of the SPD processes [12]. MDF is a repeating forging process with changes in the forging axis during MDFing by 90 degrees pass by pass [13]. Among various SPD methods, MDF seems to be most suitable for industrial production since it can be applied to relatively large samples. Multi-axial forging accelerates a dense evolution of microshear bands and their intersections, which leads to the formation of misoriented domains and, therefore, grain fragmentation [14]. It is reported that the achieved grain size by MDFing of 7475 Al alloy at 523 K was about 2 μm [15]. In a similar

* Corresponding author.

E-mail address: aoba@me.tut.ac.jp (T. Aoba).

way, UFGed structures in other alloys have been successfully developed by MDFing; average grain size of 17 nm in Cu–Zn alloy by MDFing at 77 K [16]; 230–360 nm and 300 nm in AZ31Mg and AZ80Mg alloys by MDFing under decreasing temperature conditions [17,18]; 60–200 nm average (sub)grain size in a commercial purity Ti by MDFing at ambient temperature [19]; 5–10 nm grain size in SUS316L stainless steel by MDFing at 77 K [20].

As already mentioned above, age-hardening should be one of the essential keys for further strengthening of SPDed alloys. Quite a few studies about the aging behavior of SPDed 7075Al have been reported [21,22]. In the present study, changes in the microstructure and mechanical properties during artificial aging and natural aging of MDFed 7075Al are investigated. In addition, very long-period natural aging is adapted to MDFed 7075Al to evaluate sustainability. Furthermore, the differences in strengthening mechanisms, depending on aging temperature and MDFing cumulative strain, are precisely discussed.

2. Experimental

A hot-rolled plate of 7075Al with a thickness of 15 mm was cut into rectangular shaped samples with dimensions of $15 \times 15.8 \times 16.6 \text{ mm}^3$ (aspect ratio of 1: 1.05: 1.11) and was solution heat treated (STed) at 763 K for 1 h in a salt bath, followed by water quenching. The average grain size after ST was 50 μm . The sample aspect ratio was theoretically determined for MDFing by employing pass strains of $\Delta\epsilon = 0.1$. Seven passes of MDFing, i.e., cumulative strain of $\Sigma\Delta\epsilon = 0.7$ at maximum, was applied to the samples at room temperature (RT) on an Amslar-type mechanical testing machine at an initial strain rate of $3 \times 10^{-3} \text{ s}^{-1}$. MDFing was conducted right after ST. Samples were isothermally aged at RT (natural aging) and at 393 K (artificial aging).

The change in hardness during aging was measured using a micro-Vickers hardness (HV) tester by applying a load of 300 g for 15 s. Before measurement, sample surfaces were mechanically and chemically polished. Tensile specimens with a gauge length of 6 mm and a cross sectional area of $2.0 \times 0.8 \text{ mm}^2$ were discharge-machined. The tensile test was conducted on an Instron-type mechanical testing machine at an initial strain rate of $3 \times 10^{-3} \text{ s}^{-1}$ at RT. Three samples were tensile tested for each MDFing and aging condition.

Macroscopic structure was observed using optical microscopy after mirror surface finishing by mechanical and electrical polishing, and then etching by the Keller solution. Substructures and precipitates were observed using transmission electron microscopy (TEM; JEOL JEM-2100F) at an accelerating voltage of 200 kV. The TEM foil samples were prepared by twin-jet electropolishing (Struers Tenupol-5) with a solution of 25% nitric acid and 75% methanol at 243 K. Foil thickness was determined from the convergent beam diffraction pattern [23,24]. Number density and particle size of precipitates were evaluated from TEM images using ImageJ software [25].

Phase identification of precipitates and measurement of dislocation density were conducted by means of X-ray diffraction (XRD; Rigaku RINT-2500, Cu-K α radiation at 60 kV and 300 mA). Dislocation density was estimated by employing the conventional Williamson–Hall relationship [26].

3. Results and discussion

3.1. Changes of mechanical properties by MDF and aging

Fig. 1 shows a series of stress-strain curves obtained during MDFing of 7075Al. It can be seen in Fig. 1 that the flow stress increased rapidly during the pass by pass of MDFing. Yield stress also increased rapidly at the lower cumulative strain region and gradually at the high cumulative strain region with an increasing cumulative strain. No macroscopic structural changes were observed before and after MDFing.

The age-hardening curves of 7075Al MDFed to different cumulative strains of 0, 0.3, 0.6 and 0.7 are presented in Fig. 2. Please note that the

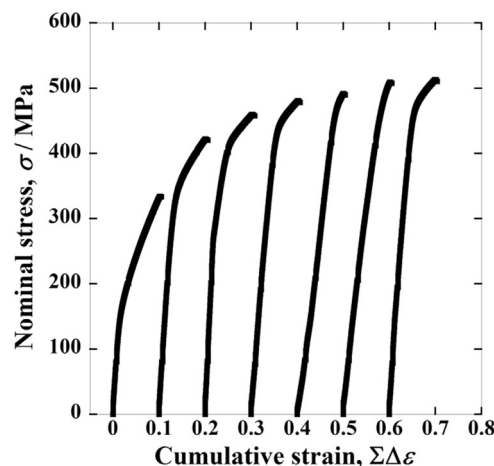


Fig. 1. Typical nominal stress-cumulative strain curves obtained during multi-directional forging of 7075Al alloy at room temperature.

time scales of both figures are quite different. The longest natural aging time was 2.4 years. The hardness of the as-STed sample was 125 HV, whereas in the as-MDFed sample it increased up to 150 HV, 170 HV and 175 HV with cumulative strains of 0.3, 0.6 and 0.7, respectively. An increment in hardness during both the artificial and natural aging of the STed sample appeared earlier than in the MDFed samples. Obvious softening took place at the beginning of artificial aging of the MDFed samples. This softening followed by age-hardening resulted in much sharper age-hardening curves compared with those obtained by natural aging. The softening was more significant in the samples MDFed to higher cumulative strains. Therefore, the increment in the hardness of the MDFed samples during artificial aging was retarded due to the accompanied occurrence of softening. In other words, softening induced by recovery exceeded the effect of age-hardening at the beginning of artificial aging. It should be noted that the aging time to attain peak hardness becomes shorter and the reduction in hardness of the MDFed samples took place earlier and more rapidly with increasing cumulative strain. It is interesting to note, however, that the achieved peak hardnesses were almost comparable (i.e. approximately 185 HV) when aged artificially.

On the other hand, natural age-hardening behavior appears quite different from that during artificial aging. The hardness increment in the MDFed samples by natural aging was rather small and furthermore becomes less significant with increasing cumulative strain. The peak hardnesses of the MDFed samples, however, were almost comparable with those achieved by artificial aging, whereas the amount of age-hardening in the natural-aged STed sample is approximately half of that in the artificially aged one.

Fig. 3 shows the typical stress-strain curves obtained by tensile tests of the samples STed and MDFed to $\Sigma\Delta\epsilon = 0.7$ all followed by peak-aging. The measured mechanical properties are summarized in Table 1. The yield and ultimate tensile strengths of the STed sample were lowest while total elongation was the largest among the samples tensile tested. Artificial aging at 393 K for 80 ks (see Fig. 2(a), peak-aged) of the STed sample derived a preferable balance of mechanical properties. However, it is well known that a problem of stress corrosion cracking arises in 7075Al prepared by this heat treatment process [4]. The amount of strengthening by natural aging of the STed sample for 7800 ks (peak-aged) was rather small. MDFing of the STed sample increased yield and ultimate tensile strengths almost comparable to those of the natural aged STed sample while total elongation decreased. Aging of the MDFed sample increased yield and ultimate tensile strengths even further. Artificial aging at 393 K for 26 ks (peak-aged) of the MDFed sample recovered ductility to 9% in addition to strengthening the yield and ultimate tensile strengths up to 498 MPa and 540 MPa respectively. In contrast, natural aging of the MDFed sample for 7800 ks (peak-aged)

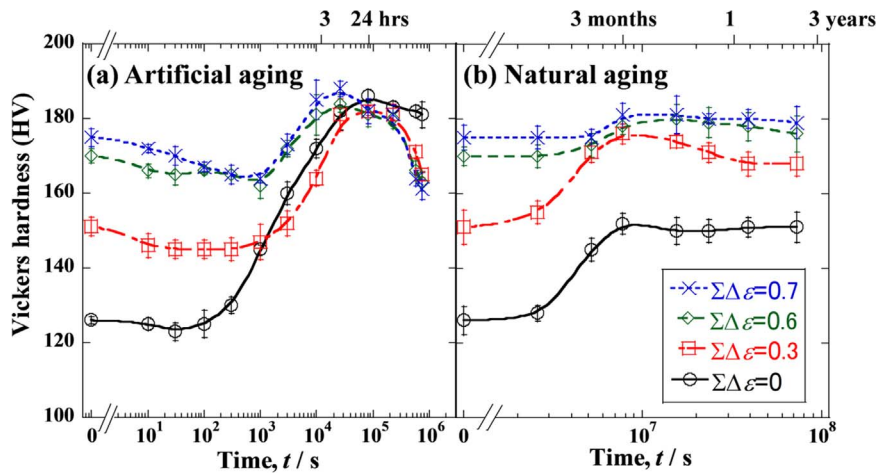


Fig. 2. Change in the Vickers hardness of the multi-directionally forged 7075Al alloys during aging at (a) 393 K and (b) room temperature.

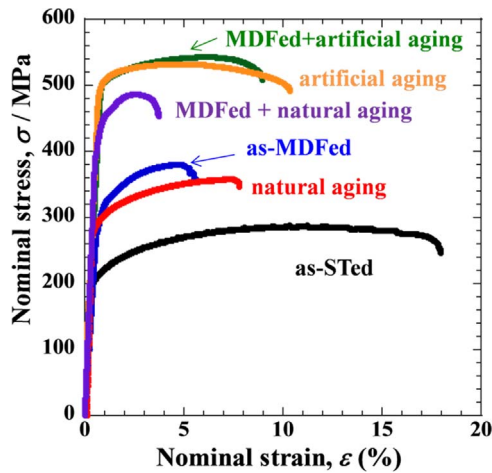


Fig. 3. Nominal stress vs. nominal strain curves obtained by tensile tests of various samples (solution heat treated: STed, multi-directionally forged: MDFed) followed by aging at 393 K for 7800 ks or at room temperature. All aged samples were those of peak aged as shown in Fig. 2. All the MDFed samples were STed in advance.

Table 1

Mechanical properties obtained by tensile tests of the 7075Al alloys with or without multi-directional forging (MDFing) before artificial or natural aging. Amount of relative increase in strength (inc.) is also described for comparison.

	0.2% Yield strength, σ_{ys} MPa (inc.)	Ultimate tensile strength, σ_u MPa (inc.)	Total elongation %
as-STed	205 (+ 0)	285 (+ 0)	18
as-MDFed	301 (+ 96)	379 (+ 94)	6
ST + artificial aging at 393 K	500 (+ 295)	530 (+ 245)	11
MDF + artificial aging at 393 K	498 (+ 293)	540 (+ 255)	9
ST + natural aging at RT	293 (+ 88)	361 (+ 76)	8
MDF + natural aging at RT	395 (+ 190)	485 (+ 200)	4

reduced ductility down to 4% and strengthening was lower than those artificially aged.

3.2. Change in microstructure by MDF and aging

Fig. 4 displays the XRD patterns of the STed and MDFed samples before and after aging at RT for 7800 ks and at 393 K for 26 ks (peak aged). The XRD analysis of the as-STed sample revealed the peak of

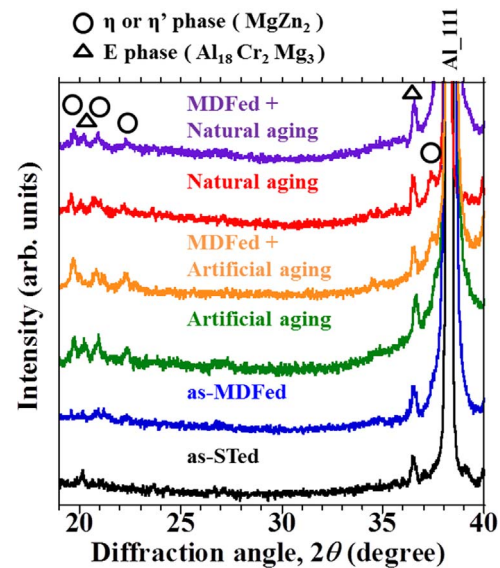


Fig. 4. XRD patterns for the samples solution heat treated (STed) and multi-directionally forged (MDFed) to cumulative strain of $\Sigma\Delta\epsilon = 0.7$. Some samples were followed by aging at room temperature and 393 K. Peaks of the η and/or η' [4] and E [28] phases are indicated by circle and triangle symbols, respectively.

non-dissolved $\text{Al}_{18}\text{Cr}_2\text{Mg}_3$ phase as well as major Al matrix, where the phase has a diamond structure and is called E phase [27,28]. After aging, some new peaks further appeared and were characterized as stable η or metastable η' phases having the same chemical composition (MgZn_2) but with slightly different lattice parameters; the η and η' phases have a hexagonal structure with $a = 0.521$ nm, $c = 0.860$ nm and $a = 0.496$ nm, $c = 1.402$ nm [2], respectively. Their overlapped peaks in the XRD patterns made definite identification of the precipitates difficult [29]. The broad peaks of the XRD pattern around 20 degrees may suggest the potential presence of GP zones [6]. However, it was difficult to confirm the presence of GP zones because of the too low intensities of the corresponding peaks. A GP zone was not detected even by precise TEM observations. With increasing aging time, the diffraction peaks of η and/or η' phases became sharper and more evident indicating growth and an increase in the volume fraction of them. On the other hand, in the as-MDFed sample, a small peak of these precipitates could be evidently detected. It has been established that 7xxx alloys are prone to dynamic precipitation when deformed from an as-STed state [11]. This would be presumably because of accelerated precipitation due to high dislocation density and a slight temperature increase during MDFing. It is also to be noted that the sharp peak around 20 degrees in the as-STed sample, which comes from the E phase, decayed after

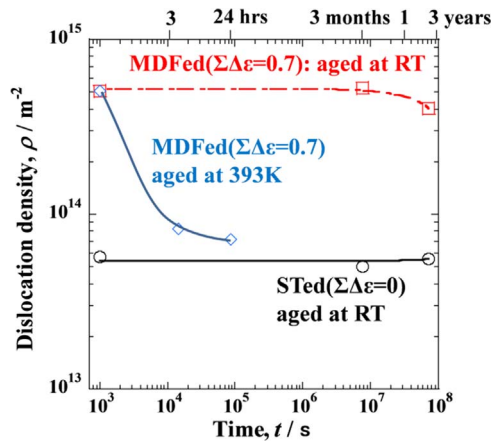


Fig. 5. Change in the dislocation density during natural aging of the solution heat treated (STed) and multi-directionally forged (MDFed) samples, together with the results of the MDFed sample aged at 393 K.

MDFing. The result suggests that the dynamic dissolution of E phase occurred during MDFing. No clear difference was found between the XRD patterns of the as-STed and MDFed samples after natural aging for 2.4 years. The peak intensity of the η and/or η' precipitates after artificial aging are evidently higher than that after natural aging, which suggests a change in precipitation behavior depending on temperature. This will be shown later in Fig. 6.

Changes in dislocation density in the samples during aging at 373 K were estimated by means of XRD and the summarized results are shown in Fig. 5. The dislocation density in the sample MDFed to $\Sigma\Delta\epsilon = 0.7$ was one order in magnitude higher than in the STed one. The dislocation densities of the as-STed and MDFed samples were almost unchanged during natural aging for 2.4 years, while in the MDFed one it rapidly dropped by artificial aging at 393 K.

Typical TEM bright field images of the MDFed samples followed by peak aging are shown in Fig. 6. Precipitates were observed to uniformly distribute. Typical TEM images with corresponding diffraction patterns of precipitates for the structural analyses are displayed in Fig. 7. From the analyses, the diffraction patterns and the power spectrums, they were identified as E, η and η' phases. The results are analogous to the

previous reports [2,3,28]. While both coarse η and fine η' precipitates were observed in all tested conditions, the density of the η' precipitates appeared much higher than that of the η ones. Furthermore, the presence of GP zones was not detected at any of the natural aging conditions after MDFing. Therefore, the potential presence of GP zones, which may also affect the mechanical properties, should be ignored. The microstructure developed in the simply artificial-aged sample without MDFing (i.e. ST + artificial aging) was a typical one observed in A7075 alloy with T6 temper [30] in which spherical η' precipitates with a size of several nanometers are homogeneously distributed. In the natural-aged sample without MDFing (i.e. ST + natural aging), on the other hand, further finer η' precipitates were observed. The density and averaged radius of the η' precipitates are summarized in Table 2. Both are obviously higher and larger when artificially aged compared with those naturally aged. A low magnification TEM image of the MDFed sample shown in Fig. 8 revealed the formation of a dislocation substructure. The subgrain size ranged roughly between 0.5 and 3 μm . The higher dislocation density introduced by MDFing would induce more inhomogeneous nucleation and partial growth of the η' precipitates lain on dislocations while it decreased number density. This tendency seemed to be more apparent by artificial aging.

3.3. Strengthening mechanisms by MDF and aging

Additional strengthening of MDFed 7075Al involving age-hardening was successfully carried out. The most dominant and effective strengthening mechanisms are dislocation hardening and precipitation strengthening in the present thermo-mechanical process. Osamura et al. experimentally showed that the dislocation bypass mechanism of particles in 7475Al alloy changed from shearable to non-shearable i.e., to Orowan looping when the radius of precipitates became over 2 nm [31]. All the precipitates observed in the present study were much larger than 2 nm. Precipitation strengthening $\Delta\sigma_p$ can be calculated on the basis of the Orowan looping mechanism using the following equation [32,33].

$$\Delta\sigma_p = \frac{0.4GbM}{\pi\sqrt{1-\nu}} \frac{\ln(2\bar{r}/b)}{\lambda} \quad (1)$$

Where ν the Poisson's ratio is equal to 0.33 for Al alloys, \bar{r} the mean radius of a circular cross section in a slip plane for a spherical

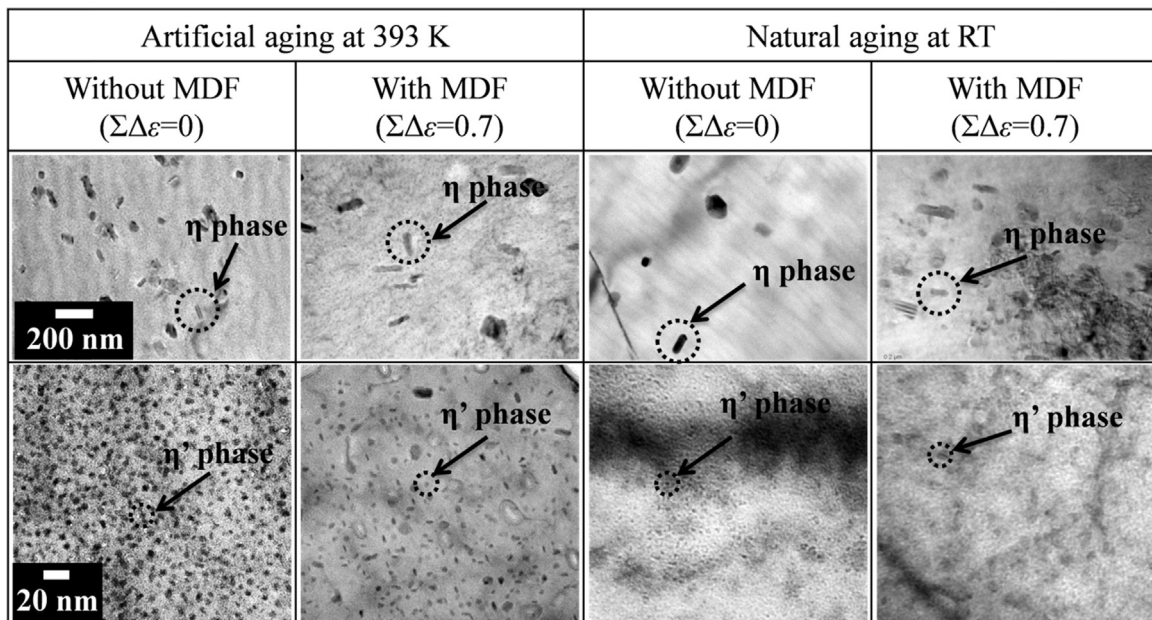


Fig. 6. Bright field images of the samples solution heat treated (STed, i.e. $\Sigma\Delta\epsilon = 0$) and multi-directionally forged (MDFed) to $\Sigma\Delta\epsilon = 0.7$ followed by peak aging at 393 K and room temperature (see Fig. 2).

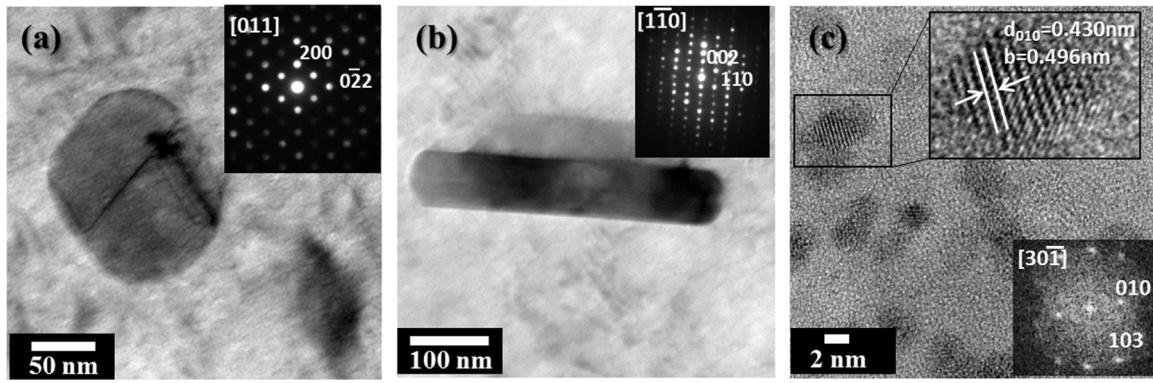


Fig. 7. Samples of typical TEM images employed for structural analyses of (a) E, (b) η and (c) η' phases: The corresponding electron-diffraction patterns of the precipitates are also shown in (a) and (b). In (c), a further enlarged image and the power spectrum obtained by the fast Fourier transform analyzer are displayed.

Table 2

Statistical summary of the distribution of η' precipitates in the samples after natural aging and artificial aging to peak hardness, together with strengthening factors estimated from the results of tensile tests and those calculated from Eqs. 1 and 3.

	Artificial aging at 393 K		Natural aging at RT	
	without MDF ($\Sigma\Delta\epsilon = 0$)	with MDF ($\Sigma\Delta\epsilon = 0.7$)	without MDF ($\Sigma\Delta\epsilon = 0$)	with MDF ($\Sigma\Delta\epsilon = 0.7$)
Number density of η' ($10^4/\mu\text{m}^3$) ^a	12	7	2.4	1.9
Precipitates radius of η' (nm)	2.3(4) ^b	4(1)	1.6(5)	3.4(8)
Precipitates volume fraction of η' (vol%)	0.54	0.36	0.050	0.14
Precipitation hardening, $\Delta\sigma_p$ (MPa)	260	280	78	120
Dislocation hardening, $\Delta\sigma_d$ (MPa)	–	24	–	100
$\Delta\sigma_{d \& p}$ (MPa) ^c	260	281	78	156
Change in yield stress, σ_{ys} (MPa) ^d	295	293	88	190

^a Foil thickness was determined from convergent beam diffraction pattern [23,24].

^b Numbers in the brackets indicate experimental errors.

^c Value defined by $\Delta\sigma_{d \& p}^2 = \Delta\sigma_d^2 + \Delta\sigma_p^2$ [24].

^d Difference in the yield stresses between aged and as-solution heat treated (STed) samples.

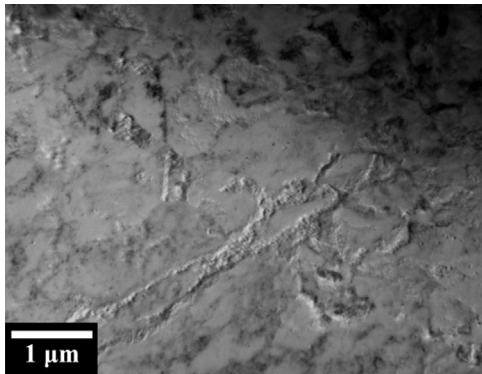


Fig. 8. Bright field image of 7075Al alloy multi-directionally forged (MDFed) to a cumulative strain of $\Sigma\Delta\epsilon = 0.7$.

precipitate, λ the inter-precipitate spacing [34].

$$\lambda = r \left(\sqrt{\frac{2\pi}{3f}} - 1.63 \right) \quad (2)$$

Where f is the volume fraction of precipitates and r is described using mean radius of precipitates r .

$$\bar{r} = \sqrt{2/3} r \quad (3)$$

The calculated $\Delta\sigma_p$ values in this way are shown in Table 2. The value was much reduced by natural aging compared with artificial aging of alloys with and without MDFing. This was caused by prevention of growth and, in particular, reduction of the volume fraction of precipitates (see Table 2).

The dislocation hardening $\Delta\sigma_d$ was calculated by the Bailey-Hirsch equation [35] as follows.

$$\Delta\sigma_d = M\alpha Gb\sqrt{\rho} \quad (4)$$

Where ρ measured dislocation density, M the Schmid's orientation factor equal to 3.06 for the FCC polycrystalline material, α a constant value of 0.2 for FCC structure, G the shear modulus of Al matrix phase equal to 26.9 GPa and b the Burgers vector equal to the lattice parameter of 0.286 nm. The estimation provides $\Delta\sigma_d = 260$ MPa and 78 MPa in artificial aging and in natural aging respectively, which corresponds well with the experimental values (see Table 1). In short, the calculated $\Delta\sigma_d$ values for the as-MDFed samples agree with the increment in the experimental yield stresses. Assuming the two dominant strengthening mechanisms are integrated by a superposition principle $\Delta\sigma_{d \& p}^2 = \Delta\sigma_d^2 + \Delta\sigma_p^2$ [36] (Table 2), the simple calculation of yield stress corresponds semi-quantitatively with the experimental data shown in Table 1. For strict estimation, of course, hardening due to substructure hardening, softening due to microstructural change induced by recovery, decrement in solid-solution elements and so on should be taken into account for the calculation. Dynamic precipitation might also affect the hardening [11]. In the present study, however, changes in strengths could be roughly but satisfactorily explained by using the most dominant strength mechanisms of dislocation hardening and precipitation strengthening. It is presently believed that a lower aging temperature compared with a conventional one would be favorable for improving the age hardening response of SPDed aluminum alloys [9–11]. However, the results in the present study have clearly pointed out the importance of long-term aging at room temperature (i.e., NA.) for the improvement of mechanical properties and also implied the possible change in mechanical properties during long-term service of SPD processed aluminum alloys. In summary, further systematic researches on the SPDed ones followed by aging should be expected.

4. Conclusion

The effects of natural aging for a long period of time (2.4 years) and artificial one on the mechanical properties and microstructure of 7075 aluminum alloy multi-directionally forged (MDFed) were systematically investigated. MDFing up to cumulative strain of $\Sigma\Delta\epsilon = 0.7$ raised the yield strength (+96 MPa) and ultimate tensile strength (+94 MPa) by work hardening. Additional artificial aging at 393 K for 26 ks and natural aging at room temperature for 7800 ks of the MDFed samples further successfully raised yield strengths (+293 MPa) and (+190 MPa), respectively. The mechanical properties of an MDFed sample followed by aging at 393 K were similar to those aged without MDFing. Although distinct softening took place soon after the beginning of artificial aging at 393 K, the microstructure and mechanical properties adopted by MDFing were stably maintained during natural aging for a long period of time. However, the number of precipitates in the MDFed samples was evidently smaller when introduced by natural aging compared with that by artificial aging. In the current conditions, strengthening of mechanical properties induced by MDFing and aging is dominated by precipitation and dislocation hardening.

Acknowledgements

The authors acknowledge the financial supports given by Japan Science and Technology Agency (JST) under Industry-Academia Collaborative R&D Program "Heterogeneous Structure Control: Towards Innovative Development of Metallic Structural Materials" and the Light Metals Educational Foundation, Japan.

Appendix A. Supplementary material

Supplementary data associated with this article can be found in the online version at <http://dx.doi.org/10.1016/j.msea.2017.06.017>.

References

- [1] D.A. Porter, K.E. Easterling, M. Sherif, *Phase Transformations in Metals and Alloys*, CRC Press, 2009.
- [2] X.Z. Li, V. Hansen, J. Gjønnes, L.R. Wallenberg, HREM study and structure modeling of the η' phase, the hardening precipitates in commercial Al–Zn–Mg alloys, *Acta Mater.* 47 (1999) 2651–2659.
- [3] H. Löffler, I. Kovács, J. Lendvai, Decomposition processes in Al–Zn–Mg alloys, *J. Mater. Sci.* 18 (1983) 2215–2240.
- [4] G.E. Totten, D.S. Mackenzie, *Handbook of Aluminium Volume 1 Physical Metallurgy and Process*, Taylor & Francis Inc, New York, 2003.
- [5] R.Z. Valiev, R.K. Islamgaliev, I.V. Alexandrov, Bulk nanostructured materials from severe plastic deformation, *Prog. Mater. Sci.* 45 (2000) 103–189.
- [6] M.H. Shaeri, M.T. Salehi, S.H. Seyyedein, M.R. Abutalebi, J.K. Park, Microstructure and mechanical properties of Al-7075 alloy processed by equal channel angular pressing combined with aging treatment, *Mater. Des.* 57 (2014) 250–257.
- [7] S. Lee, K. Tazoe, I.F. Mohamed, Z. Horita, Strengthening of AA7075 alloy by processing with high-pressure sliding (HPS) and subsequent aging, *Mater. Sci. Eng. A* 628 (2015) 56–61.
- [8] P.V. Liddicoat, X.-Z. Liao, Y. Zhao, Y. Zhu, M.Y. Murashkin, E.J. Lavernia, R.Z. Valiev, S.P. Ringer, Nanostructural hierarchy increases the strength of aluminium alloys, *Nat. Commun.* 1 (2010) 63.
- [9] K. Ma, T. Hu, H. Yang, T. Topping, A. Yousefiani, E.J. Lavernia, J.M. Schoenung, Coupling of dislocations and precipitates: impact on the mechanical behavior of ultrafine grained Al–Zn–Mg alloys, *Acta Mater.* 103 (2016) 153–164.
- [10] T. Hu, K. Ma, T.D. Topping, J.M. Schoenung, E.J. Lavernia, Precipitation phenomena in an ultrafine-grained Al alloy, *Acta Mater.* 61 (2013) 2163–2178.
- [11] A. Deschamps, F. De Geuser, Z. Horita, S. Lee, G. Renou, Precipitation kinetics in a severely plastically deformed 7075 aluminium alloy, *Acta Mater.* 66 (2014) 105–117.
- [12] Y. Estrin, A. Vinogradov, Extreme grain refinement by severe plastic deformation: a wealth of challenging science, *Acta Mater.* 61 (2013) 782–817.
- [13] T. Sakai, A. Belyakov, R. Kaibyshev, H. Miura, J.J. Jonas, Dynamic and post-dynamic recrystallization under hot, cold and severe plastic deformation conditions, *Prog. Mater. Sci.* 60 (2014) 130–207.
- [14] T. Sakai, H. Miura, X. Yang, Ultrafine grain formation in face centered cubic metals during severe plastic deformation, *Mater. Sci. Eng. A* 499 (2009) 2–6.
- [15] O. Sitdikov, T. Sakai, H. Miura, C. Hama, Temperature effect on fine-grained structure formation in high-strength Al alloy 7475 during hot severe deformation, *Mater. Sci. Eng. A* 516 (2009) 180–188.
- [16] H. Miura, Y. Nakao, T. Sakai, Enhanced grain refinement by mechanical twinning in a bulk Cu-30mass%Zn during multi-directional forging, *Mater. Trans.* 48 (2007) 2539–2541.
- [17] H.S. Jie Xing, Xuyue Yang, Hiromi Miura, Taku Sakai, Ultra-fine grain development in an AZ31 magnesium alloy during multi-directional forging under decreasing temperature conditions, *Mater. Trans.* 46 (2005) 1646–1650.
- [18] J. Xing, X. Yang, H. Miura, T. Sakai, Mechanical properties of magnesium alloy AZ31 after severe plastic deformation, *Mater. Trans.* 49 (2008) 69–75.
- [19] Y. Iwabuchi, Master thesis, University of Electro-Communications, 2010.
- [20] Y. Nakao, H. Miura, Nano-grain evolution in austenitic stainless steel during multi-directional forging, *Mater. Sci. Eng. A* 528 (2011) 1310–1317.
- [21] G. Waterloo, V. Hansen, J. Gjønnes, S.R. Skjervold, Effect of predeformation and preaging at room temperature in Al–Zn–Mg–(Cu,Zr) alloys, *Mater. Sci. Eng. A* 303 (2001) 226–233.
- [22] A. Deschamps, F. Livet, Y. Bréchet, Influence of predeformation on ageing in an Al–Zn–Mg alloy—I. Microstructure evolution and mechanical properties, *Acta Mater.* 47 (1998) 281–292.
- [23] S.M. Allen, E.L. Hall, Foil thickness measurements from convergent-beam diffraction patterns An experimental assessment of errors, *Philos. Mag. A* 46 (1982) 243–253.
- [24] S.M. Allen, Foil thickness measurements from convergent-beam diffraction patterns, *Philos. Mag. A* 43 (1981) 325–335.
- [25] M.D. Abràmoff, P.J. Magalhães, S.J. Ram, Image processing with ImageJ, *Biophoton. Int.* 11 (2004) 36–42.
- [26] G.K. Williamson, W.H. Hall, X-ray line broadening from filed aluminium and wolfram, *Acta Metall.* 1 (1953) 22–31.
- [27] M. Svoboda, J. Janovec, M. Jenko, A. Vrankovic, The characterisation of inter-metallic-compound particles in an annealed Al–Mg–Cr–Fe alloy, *Mater. Technol.* 38 (2004) 289.
- [28] M. Gao, C.R. Feng, R.P. Wei, An analytical electron microscopy study of constituent particles in commercial 7075-T6 and 2024-T3 alloys, *Metall. Mater. Trans. A* 29A (1998) 1145.
- [29] K. Ma, H. Wen, T. Hu, T.D. Topping, D. Isheim, D.N. Seidman, E.J. Lavernia, J.M. Schoenung, Mechanical behavior and strengthening mechanisms in ultrafine grain precipitation-strengthened aluminum alloy, *Acta Mater.* 62 (2014) 141–155.
- [30] M.H. Shaeri, M. Shaeri, M.T. Salehi, S.H. Seyyedein, M.R. Abutalebi, Effect of equal channel angular pressing on aging treatment of Al-7075 alloy, *Prog. Nat. Sci.: Mater. Int.* 25 (2015) 159–168.
- [31] K. Osamura, S. Ochiai, T. Uehara, Precipitation behavior and change of yield strength during artificial aging in Al–Zn–Mg–Cu alloys, *J. Jpn. Inst. Light Met.* 34 (1984) 517–524.
- [32] A. Kelly, R.B. Nicholson, *Progress in Metals Science*, Pergamon Press, 1971.
- [33] P.B. Hirsch, F.J. Humphreys, *Physics of Strength and Plasticity*, MIT Press, 1969.
- [34] J. Miyake, M.E. Fine, Electrical conductivity versus strength in a precipitation hardened alloy, *Acta Metall. Et. Mater.* 40 (1992) 733–741.
- [35] J.E. Bailey, P.B. Hirsch, The dislocation distribution, flow stress, and stored energy in cold-worked polycrystalline silver, *Philos. Mag.* 5 (1960) 485–497.
- [36] M.J. Starink, S.C. Wang, A model for the yield strength of overaged Al–Zn–Mg–Cu alloys, *Acta Mater.* 51 (2003) 5131–5150.